Near-optimal coverage trajectories for image mosaicing using a mini quad-rotor over irregular-shaped fields

**João Valente · David Sanz · Jaime Del Cerro · Antonio Barrientos ·
Miguel Ángel de Frutos**

Abstract Aerial images are useful tools for farmers who practise precision agriculture. The difficulty in taking geo-referenced high-resolution aerial images in a narrow time window considering weather restrictions and the high cost of commercial services are the main drawbacks of these techniques. In this paper, a useful tool to obtain aerial images by using low cost unmanned aerial vehicles (UAV) is presented. The proposed system allows farmers to easily define and execute an aerial image coverage mission by using geographic information system tools in order to obtain mosaics made of high-resolution images. The system computes a complete path for the UAV by taking into account the on-board camera features once the image requirements and area to be covered are defined. This work introduces a full four-step procedure: mission definition, automatic path planning, mission execution and mosaic generation.

Keywords Aerial images · Mosaicing · Coverage path planning · Aerial robots · Mission planner · Remote sensing

Introduction

High availability aerial vehicles equipped with inexpensive and lightweight sensors have become suitable remote sensing (RS) tools, overcoming the deficiencies of other RS options, such as satellites or airplanes. Nowadays, they are able to provide an affordable, adaptable and fast data acquisition tool for agricultural purposes.

Currently, aerial vehicles (mainly planes) are employed in agriculture for crop observation and map generation through imaging surveys (Johnson et al. 2003; Herwitz et al. 2004). The maps are usually built by stitching a set of geo-referenced images (e.g. orthophotos) through mosaicing procedures. These maps give detailed information about biophysical parameters of the crop field. The agricultural experiments reported with aerial vehicles mainly use waypoint-based navigation features (Johnson et al. 2003; Berni et al.

J. Valente (✉) · D. Sanz · J. Del Cerro · A. Barrientos · M. Á. de Frutos
Centre for Automation and Robotics (UPM-CSIC), c/José Gutiérrez Abascal, 2, 28006 Madrid, Spain
e-mail: joao.valente@upm.es

2009; Nebiker et al. 2008), where the aerial vehicles navigate autonomously through a trajectory pre-defined by a set of points in the environment.

Therefore, the aerial vehicle usually has to scan the full area by following a continuous and smooth trajectory and, at the same time, avoiding areas or parcels that are not subjects of interest.

In the light of the studies mentioned above, it can be concluded that two strongly coupled aspects have to be defined in order to accomplish the full mission: the type of UAV platform and the mission-planning solver.

Regarding UAV platforms, it needs to be pointed out that the use of planes not only intensifies the difficulty in calculating optimal trajectories but also eliminates the possibility of taking several images from the same point. In addition to this, the fact of taking pictures in motion reduces the possibility of operating in poor light scenarios, requiring high-speed image capture. Two further drawbacks in using planes compared to other vehicles are the reduction of positioning accuracy and the inability to take off or land in small spaces. On the other hand, although helicopters are a better option with regard to path planning and performance, they are highly complex and require exhaustive maintenance and extensive training for operators in order to avoid critical damage and accidents.

Quad-rotors are a novel platform that rely on the advantages of helicopters and bring together the best features for outdoor missions. This mini platform has four electric rotors but, in contrast to typical helicopters, there is no pitch blade variation. Therefore, changes in attitude or elevation are obtained only by controlling the speed of the four motors independently. As a result, quad-rotors turn out to be much easier to setup and operate than helicopters.

Additionally, considering safety aspects, the risk of material and physical injuries is less likely than with other types of mini UAVs. Finally, it is worth mentioning that quad-rotors are much cheaper than other vehicles in terms of maintenance and parts.

Currently, quad-rotors are widely available. Their high maneuverability allows reducing the time to complete their operations. As previously mentioned, path planning also has to consider suitable areas for taking off and landing to fulfill all requirements (safety margins, sufficient space for operation, pick up and drop ability, accessibility).

In order to manage these requirements, coverage path planning (CPP) techniques have been applied to solve the problem. CPP is a sub-topic of motion planning, which deals with methods to determine a path that ensures complete coverage (e.g. back and forth motions) for a robot in a free workspace.

Since the robot has to fly over all points in the free workspace, the CPP problem is related to the covering salesman problem, a NP (non-deterministic polynomial with very hard time restrictions) problem (Choset 2001). CPP with Unmanned Aerial vehicles (UAV) was discussed by Jiao et al. (2010) and Maza and Ollero (2007) where exact cell decomposition methods were proposed to break down a polygonal area.

Although the cited authors used exact cell decomposition, their approaches addressed mainly decomposition of areas and coverage with back and forth motions. This study addresses the problem of covering an entire farm site with a vertical takeoff and landing aerial robot provided with way-point navigation capability. Therefore, an off-line mission planner has been developed for commercial off-the-shelf aerial robots. The method is able to compute a coverage path that is restricted to the minimum number of turns, avoidable cells and predefined starting and goal positions.

Most UAVs employed in agricultural tasks are off-the-shelf platforms with an autopilot that is able to perform a flight following a way-point list. The work presented aims to help the operator in optimally defining a coverage mission under some usual restrictions. The mission planner computes a coverage path in a given target area and a priori information.

Since the output of the planner is retrieved as a set of geographic co-ordinates, the operator can use it with any type of aerial robot with way-point navigation features. Thus, the platform can be used by any user regardless of the level of knowledge about the system.

Previous work

In the last decade, some research has enhanced the task of acquiring aerial images by using a mini aerial vehicle. At the beginning, this task was difficult because researchers had to build the aerial platforms from basic leisure radio controlled models. These conversions were often time consuming. Moreover, the robustness of the final prototype did not comply with the required performance. Some of those achievements can be found in Xiang and Tian (2011).

Those problems have been solved with the progress in miniaturization and reduction in the cost of the system. The mini aerial vehicle market has many well-conceived off-the-shelf platforms available, which are ready to fly (both manually and using way-point navigation) and are high-level programmable (Hunt et al. 2010, Valente et al. 2011b).

Most of the reported studies have been concerned with the feasibility of the platform to acquire images or the techniques for image processing (Lelong et al. 2008; Berni et al. 2009; Hunt et al. 2010). Very few studies have focused on the ability to optimize the image survey trajectory, which is a step forward in optimizing the overall mission.

In a previous study (Valente et al. 2011), a feasible approach to survey an agricultural field subject to several constraints was proposed. It described how a coverage mission could be achieved in three steps (1. Offline definition of workspace and acquisition of data from the GIS environment. 2. Insertion and computation of coverage path based on the previous data. 3. Execution of the mission). However, no experimental results about the coverage mission were presented.

In this paper, experimental results are presented and they include a brief analysis of the results. The experimental results were obtained in a large vineyard parcel that was surveyed with a quad-rotor carrying a low cost digital camera. A low altitude flight (<100 m) was carried out in order to obtain images to build a map by using mosaicing techniques.

Mission definition

The first step of the aerial mission is the setup of vehicle and base station. In this section, the components of the system are briefly described.

Instruments and methods

The system has been split into three interconnected elements: aerial vehicle, camera and communication resources.

Maneuverability is a critical factor for the aerial vehicle. A vehicle able to move from one waypoint to another in minimal time and having the capability for hovering and backward movement is required. Additionally, an important capability for a successful execution of the mission is the possibility of hovering (staying in a determined position for some undefined time). It should also be taken into account that the mission is performed in outdoor scenarios. These missions require robust systems, capable of working under adverse weather conditions.

Multi-rotor systems comply with all these characteristics: The multiple motors of quad-rotors or hexacopters provide enough lift, not only to carry the payload, but also to hold it in different poses while performing very stable flights. At the same time, the robustness and reliability of the system are improved when uncomplicated mechanisms are used. Therefore, a four-propeller solution was selected as flying platform. Pelican quad-rotor from Ascending Technologies GmbH, which is a German company (see Fig. 1), has been used in order to perform the experiments. It has the following features:

- Maximum speed: 50 km/h
- Maximum windload: 36 km/h
- Maximum flight time: 20 min
- Maximum payload: 500 g

The second module is the image acquisition system. As previously mentioned, the drone's main mission consists of placing the camera in a set of defined locations. It requires an integration process in order to incorporate the camera in the system, both mechanically and electronically: On the one hand, the mechanical integration aims to hold the camera at the front side of the drone, pointing downwards. It has entailed the design of a specific element, ergonomic and robust enough to guarantee the security of the assembly. Nevertheless, this necessary component places the camera away from the drones' center of gravity (CoG). Due to this, the quad-rotor attitude should be projected so as to estimate its effect on deviation in the acquired image by using Euler angles. Equation 1 presents the required transformations:

$$
T = Rot_{roll}(\alpha) * Rot_{pitch}(\beta) * Transl\left(P_{x,y,z}\right) =
$$

$$
\begin{bmatrix}
\cos(\beta) & 0 & \sin(\beta) & P_x \\
\sin(\alpha) * \sin(\beta) & \cos(\alpha) & -\cos(\beta) * \sin(\alpha) & P_y \\
t - \cos(\alpha) * \sin(\beta) & \sin(\alpha) & \cos(\alpha) * \cos(\beta) & P_z \\
0 & 0 & 0 & 1
\end{bmatrix}
\tag{1}
$$

where α and β represent the roll and pitch absolute angles, and $P_{x,y,z}$ is a three co-ordinates vector, which describes the distance from the CoG of the quad-rotor to the CoG of the

Fig. 1 Quad-rotor with the embedded on-board camera

camera. In this study, this equation should be substituted with the following values: $P_x = 0$ m, $P_y = 97$ mm and $P_z = -20$ mm.

The selection of the camera should also be considered. In this sense, the mission sets several requirements: Firstly, the weight has to be as low as possible. Furthermore, the lenses should be able to work in poor light scenarios. It will therefore need large sensors, which are two conflicting requirements. The images are captured whilst the drone is in motion. Therefore, a fast shutter speed is required in order to minimize this effect and obtain clearer and sharper photographs. Nevertheless, the higher the shutter speed is, the lower the illumination of the scene. Therefore, high brightness lens are required to compensate for this effect. Since a trade-off was required, a PENTAX Option S1 has finally been chosen. It has the following characteristics:

- Dimensions: $90 \times 54 \times 20$ mm
- Weight: 110 g
- Lens: 28–140 mm (35 mm equiv.). f/3.9–5.7
- ISO sensitivity: 64 to 6 400 ISO
- Maximum image resolution: $4\,288 \times 3\,216$ pixels
- Resolution: 14 M pixel
- Sensor: CCD 1/2.3 in
- Maximum shutter speed: 1/6 000 s
- Image stabilizer: Yes (optical)
- Video recording: HD 720p

Finally, when evaluating and designing the system, the control modes and the command exchange protocol should be taken into account. Thus, a remote control to operate the camera is required. PENTAX Option S1 and its IR handler have been analyzed. The camera's protocol has been decrypted (see Fig. 2) and replicated in an on-board device. It uses an independent full-duplex XBee channel, which is connected to the base station, in order to allow the camera to be triggered both manually and automatically. In this second mode—the predefined one—the system analyzes the quad-rotor navigation data provided by the controller, and commands the acquisition according to the quad-rotor position, attitude and speed. Since the images are acquired only when the attitude values are below a predefined threshold, a minimum error in the correspondence between the images and the position where they were taken can be guaranteed.

The integration—as well as the control—were implemented using the robot operating system architecture and resources (Quigley et al. 2009). It allows using a modular implementation that directly connects the drone's navigation data with the triggering decider process. It also provides a fast response that enables quick geo-referencing by matching images with the navigation data.
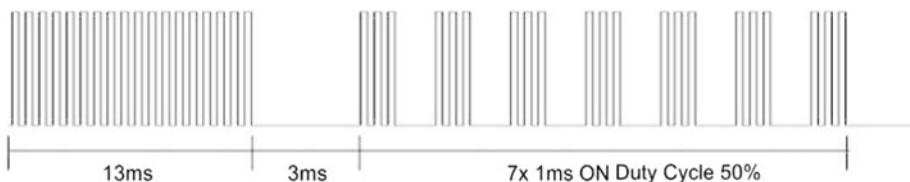

Fig. 2 IR remote control for PENTAX Option S1 triggering. The sample frequency is 38 kHz 8

Workspace sampling

The environment has been modeled through an approximate cellular decomposition following the taxonomy proposed by (Choset 2001), which means that the robot workspace is sampled as a regular grid. The grid-based representation with optimal dispersion is obtained by dividing the space into cubes and considering their centers as waypoints for the drones. This arrangement can be considered as a kind of Sukharev grid (LaValle 2006). It should be highlighted that exact cell decompositions such as trapezoidal decompositions are inefficient for aerial coverage, since the goal is to acquire a homogeneous sized set of samples with the same spatial resolution from the target environment. This is not possible to be obtained using a fix focal length camera as shown in Fig. 3, where the exact cell decomposition on the right provides a set of irregular cells that do not correspond to the shape of an image frame. In this method, the cells homogeneity is not ensured.

Grid-based representations provides a simple way to manage this problem, since the center of each cell is assumed to be a way-point, and the cell dimension is proportional to the image dimension obtained from the visual sensor.

The grid resolution is obtained through image requirements—resolution and overlapping—and the image sensor characteristics. The first step is to determine a desired spatial resolution (pixels/m). By using this parameter and the real resolution of the available camera, the cell dimension can be computed. This spatial resolution depends on the final use of the picture (water stress, weed detection, etc.). Since the real size of the cell and the dimensions of the ground are known, the number of cells (actually photographs) required to map the whole field can be easily computed. Finally, the last parameter to be computed is the flight altitude in order to ensure the cell dimensions (photograph dimensions projected from the ground). The aerial vehicle height above the ground can be computed through the relationship shown in Eq. 2.

$$\frac{T_d}{T_h} = \frac{I_d}{l} \tag{2}$$

where τ_d, τ_h, I_d, l stand respectively for target dimension, target distance, image dimension, focal length of the camera (see Fig. 4). After that an offset $\delta < 0$ is added to the computed co-ordinates in order to apply the overlapping rate.
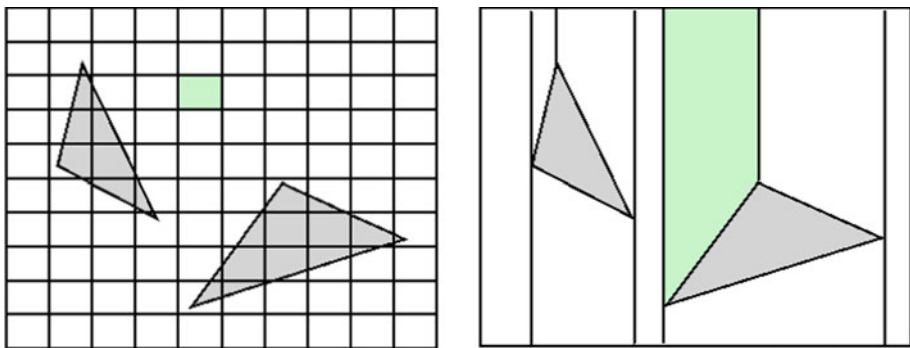

Fig. 3 An environment decomposed by two different methods. For each workspace, a cell is highlighted in *green* (Color figure online)
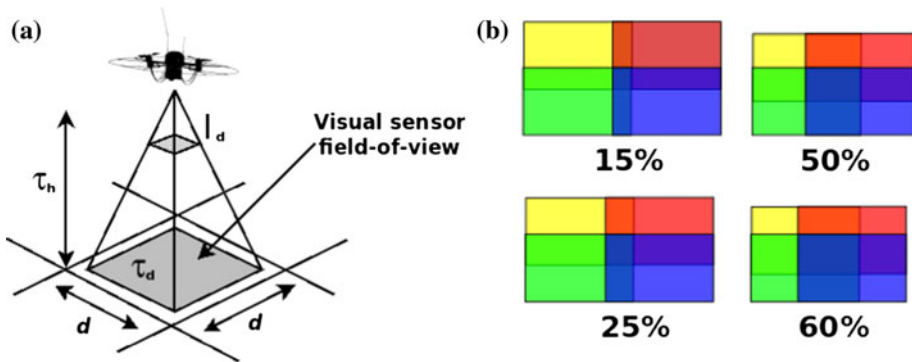
Fig. 4 Aerial height computation during the mission. **a** Ground cell dimensions and aerial vehicle height relationship. **b** Image overlapping rates obtained with different δ

Path generation

After the mission definition previously addressed, the next step is to compute the aerial coverage trajectory. This step is mainly addressed by the mission planner: first, convert the decomposed workspace to a regular graph and then compute the coverage path by employing graph search approaches.

Workspace to graph conversion

Consider a square or rectangular area $\Phi \subset \Re^2$ and approximately decomposed by a finite set of regular cells $C = \{c1...cn\}$ in such way,
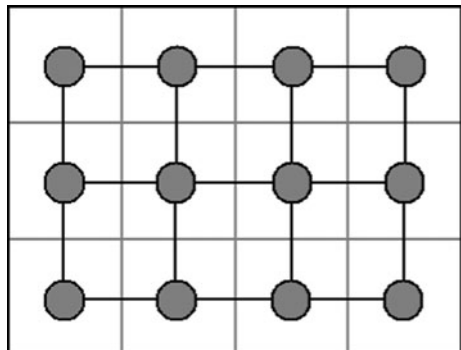
$$\Phi = \bigcup_{c \in C} c \tag{3}$$

One of the big advantages of having a grid-based decomposition is that the robot workspace can be directly converted into a kind of unit distance graph, denoted as grid graph (see Fig. 5), and that can be written as,

$$G_{\langle V,E \rangle} \quad \text{where } v = p, v \in V \text{ and } p \in \mathbf{P} \tag{4}$$

where V are the vertex, E the edges. $\mathbf{P}$ is a discrete trajectory defined by way-points, such that,

Fig. 5 A grid graph

$$\mathbf{P} = \bigcup_{p \in \mathbf{P}} p \tag{5}$$

Each vertex represents a way-point and each edge, the path between two way-points u and v such that $u \sim v$.

CPP

Heuristic and non-heuristic algorithms have been employed to obtain a complete coverage path with the minimum number of turns, subject to a pre-defined initial and goal position and without re-visited points within the workspace.

The distance transform function is applied over the grid by employing a Bread-first search (LaValle 2006) on the graph induced by the neighborhood adjacency of cells. As a result, the coverage path can be easily found from any starting point within the environment to the goal cell by choosing the nearest neighbor cell in gradient ascendant order instead of the common descendant order.

Deep-limited search (LaValle 2006) is used to build a tree with all possible coverage paths in order to find a complete coverage path that passes through all nodes in the adjacency graph only once. Using this approach, the search length can be limited to the number of vertices, and consequently, the search neither goes around in infinite cycles nor visits a node twice.

During the gradient tracking, the algorithm will find more than one neighbor to choose from with the same potential weight. Additionally, the bottleneck caused by the local minimum can also block the search. In order to solve these issues, a backtracking procedure was employed.

Finally, the coverage path with the minimum number of turns is chosen by using the following cost function,

$$\Gamma = \sum_{i=1}^{m} \gamma_k^{\{i\}}, \quad k \in \{135^\circ, 90^\circ, 45^\circ, 0^\circ\} \tag{6}$$

where,

$$\gamma \pm 135^\circ > \gamma \pm 90^\circ > \gamma \pm 45^\circ > \gamma 0^\circ \tag{7}$$

The algorithm pseudo code is shown in Algorithm 1, where Φ is a field sampled in a finite number of way-points, $\mathbf{P}$ is a complete coverage path.

Algorithm 1 Coverage path planning algorithm

```
1: Initialize FiFo = ∅
2: G_<V,E> ← ConvertToGraph(Φ)
3: G'_<V,E> ← Wavefront(G_<V,E>)
4: while ∃P ∈ Φ do
5:     P ← DLS_w/Backtracking(G'_<V,E>)
6:     FiFo ← FiFo + P
7: end while
8: P* ← min(Γ(FiFo))
9: Return P*
```

The gradient-based approach, although not ensuring an optimal solution, provides a simple and a rapid way to obtain a near optimal coverage solution, in both regular and irregular fields, with and without obstacles, subject to the aforementioned restrictions.

Results

Finally, the mission execution is carried out. In this section, the experimental results concerning the image survey mission with a quad-rotor carrying a digital camera are presented. The agricultural field chosen to put the aforementioned approach in practice is a vineyard parcel located in Belmonte de Tajo, near Madrid, Spain. The agricultural field with irregular shape is shown in Fig. 6.

Aerial coverage

In order to plan the coverage mission, a geo-referenced image from the target field should be obtained from a GIS database. The orthophoto used in planning the mission is depicted in Fig. 7. The following areas have been delimited: (1) workspace boundaries (solid yellow), (2) field boundaries (solid blue), (3) undesired patches (dashed red). Further non-interest areas inside the workspace are pointed out with dashed red arrows.

The workspace is then decomposed considering its properties, the mosaic requirements and the digital camera parameters according to the methods described in the section Mission definition. Those values are summarized in Table 1.

The aforementioned values provide sufficient information to compute the number of cells in which the workspace is decomposed. The real size of each cell and the height above the ground are required to ensure the previous requirements. Thus, the real size of the cells projected on the ground is computed by using the values from Table 1a, b, resulting in squared cells with 32.16 m sides. The number of photographs required to map the agricultural field are obtained by taking into account this value and the information given in the Table 1c. Therefore, the workspace is decomposed into 60 cells (6 × 10). Finally, the last parameter to be obtained is the quad-rotor flight altitude, which is computed by applying Eq. 2, the values from Table 1b and the previous computed real cell size τ_d. The altitude τ_d computed turned out to be 45.94 m ($\sim$46 m).

Fig. 6 Vineyard parcel of area approximately 63,765 m^2 (195 × 327 m) and geographic co-ordinates 40°06′47.43″N and 3°17′02.33″W

**Fig. 7** Workspace definition inside the agricultural field

Moreover, as there are areas that do not need to be covered, it means that there are points with no information of interest. They are points where the quad-rotor does not have to pass. These points could be a pond, a patch without cultivation or with some kind of agricultural infrastructure or machinery inside. After defining which are and which are not the points within the environment to be considered for mapping, the mission planner computes the flight trajectory as detailed in the section Path generation.

The vineyard parcel is shown decomposed in a grid-based fashion in Fig. 8. From 60 cells, 25 % were not considered in the coverage trajectory. The coverage path was computed by considering initial and final positions, which are typically near the base station where all equipment and ground personal are located. The red square on the picture depicts the base station location in the grid. Furthermore, the blue dotted line represents a small trajectory carried by the quad-rotor after finishing the coverage mission and coming to the initial (as well as the final) point of the mission (return home procedure).

The coverage trajectory depicted in Fig. 8 can be sent to the quad-rotor and then the mission is carried out. In addition to the X and Y co-ordinates, the Z has to be set corresponding to the computed height. An offset of 9 m was added to the vehicle height in

Table 1 Mapping values considered in the workspace decomposition	(a) Mosaic requirements		
	Spatial resolution		Image overlapping
	10 mm/pixel		5 %
	(b) Digital camera characteristics		
	Image resolution	I_d	l
	10 M (3,216 × 3,216 pixels)	35 mm	50 mm
	(c) Workspace size		
	Width		Length
	195 m		327 m

Fig. 8 Path generated by the mission planner
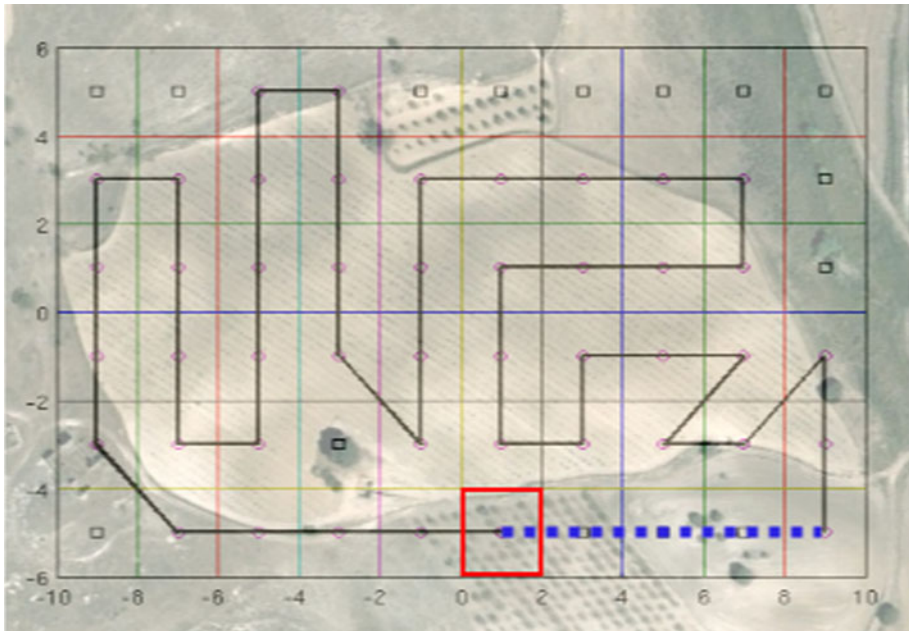
order to compensate height estimation accuracy and ensure overlapping rate. Moreover, cruise speed was set to 3 m/s. The real trajectory performed by the quad-rotor is shown in Fig. 9 (blue solid line). The resulting coverage path relies on 21 turns with predefined start and goal positions. The overall heading rotation cost can be expressed as,

$$\Gamma = 4 \times \Gamma_{135°} + 13 \times \Gamma_{90°} + 4 \times \Gamma_{45°} + 28 \times \Gamma_{0°} \qquad (8)$$

The overall coverage mission was accomplished in 660 s, with 82 % of effective aerial coverage and 18 % of system assessment and ground station setup. A set of metrics obtained after flight is summed up in Table 2.

Typical coverage patterns denoted as Serpentine or Back-and-forth motions are often used in agriculture since they are easy to compute. However, they become inefficient trajectories when irregular shape fields are considered.

In order to evaluate the reduction in time required for the coverage by using different types of planners, three different solutions have been considered. A basic Serpentine algorithm, a "smart" serpentine algorithm (that takes into account the returning home path in order not to repeat some waypoints) and finally, the proposed approach.

Considering the mission time required by the basic serpentine algorithm as reference, the smart serpentine has achieved a reduction of 14 % and a reduction of 27 % for the proposed algorithm. The number of cells without interest that the drone visited using basic serpentine algorithm was 15 %. Nevertheless, this number strongly depends on the shape of the field.

Furthermore, the main advantage of the proposed algorithm is not only the reduction in mission time but also the flexibility for its use in large areas with irregular shapes. These areas can include points of no interest such as greenhouses, lakes or rivers. The proposed approach allows the drones to perform their task in a fully automated manner and reduce the time that drones are out of the target field to a minimum.

Fig. 9 Quadrotor real flight trajectory over the vineyard parcel

Table 2 Results obtained in the coverage mission

Metrics measured after flight					
Turns	Coverage time (s)	Setup time (s)	Path length (m)	Height (m)	Speed (m/s)
21	540	120	1,546	55	3

Image acquisition and mosaicing

In the last stage of the process, all resources generated in previous phases have to be combined. As a result, a global image of the current environment could be obtained by joining the set of images acquired during the flight. Nevertheless, due to the errors set by the real operation, a sequential combination of the photographs is not enough. In order to get good performance, both image pre-processing and post-processing are necessary. On the other hand, accurate methods are usually complex and slow. They do not allow real time responses, as needed for example in robot co-operation. Thus, a method to increase handling speed is advisable. In order to achieve this, a refinement process has been implemented in four simple steps. It takes advantage of their individual simplicity for providing a faster response.

The first step starts with navigation data analysis that allows performing the initial image alignment: whenever a photograph is taken, the quad-rotor associates the information in the flight registers with the picture acquired at that moment. These data, provided by the Flight Control System, are not only made of GPS co-ordinates, but also orientation and attitude estimation. Despite errors and bias, the correlation of this information allows placing every photograph in a relative sketch. Figure 10 presents the results obtained in the first approach. Although the images are correctly placed, it can be observed that many crop rows do not match. That is due to the measurement and calibration errors, which are inherent to the system.

Fig. 10 Photographic superposition based only on the flight data provided by the quad-rotor. On the *left*, image borders are shown in order to highlight the position and orientation of each one. On the *right*, the resulting image where no correspondence in rows can be appreciated

The definition of a maximum error allowed threshold imposes the maximum displacement on the mosaicing process. Additionally, it could also be observed that different exposure levels make matching process and posterior identification attempts difficult.

The second step consists of rectifying the deformations and distortions derived from the drone's attitude in the acquisition time: non-zero roll and pitch angles require a projection correction in order to compensate the vertical drift. In such manner, the acquisition height has to be considered since projection error is directly related to the flight altitude.

The correction has been done using PanoTools and Hugin's Batch Processor algorithm (German et al. 2007). This method warps each image according to its attitude parameters. An equi-rectangular approach has been chosen, with a horizontal field of view (HFOV) of 67.9 and a barrel factor of 0.00005. Table 3 summarizes the angles estimated for five continuous photographs. The corrections, adapted according to Philpot (2001), prompt a collection of overlapped images (see Fig. 11), which are the starting point for the third step.

After correcting the distortion, the resulting image has to be remapped on the tangent plane, avoiding the lens deviation. Considering that almost all deviations occur radially, towards or away from some common center, a radial correction was applied considering the following third degree polynomial for describing the distortion:

$$r_{src} = \left(ar_{dest}^3 + br_{dest}^2 + cr_{dest} + d\right)r_{dest} \qquad (9)$$

where r_{src} and r_{dest} refer to the normalized radius of an image pixel (source and destiny radius, respectively). The values of the parameters that resolve $r_{src} = r_{dest}$ were obtained experimentally: $a = 0.22886$, $b = -0.42509$ and $c = 0.37991$. The 'd' parameter was omitted since it is related to the aspect ratio.

Table 3 Correction parameters for quad-rotor's attitude compensation

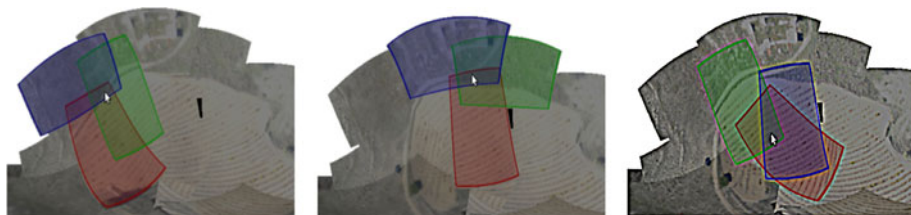| Image	Yaw	Pitch	Roll	EV
0	−0.052	−0.002	0.986	13.3
1	72.176	0.04	1.015	13.2
2	33.76	0.035	1.505	13.1
3	35.43	0.119	1.135	13.8
4	34.64	0.008	1.055	13.6

Fig. 11 Three examples of different stitching steps. The image set used in each step is highlighted in *different colors* (Color figure online)

In the same way, the second step implies an adjustment in terms of photometry (Philpot 2001): The exposure and white balance are adapted in each image in order to generate a homogeneous composition. Table 3 column 4 shows the exposure value (EV) calculated for five consecutive images. It has been used as an EMoR (empirical model of response).

In addition to this, other effects make difficult the association process, such as the vignetting effect (Aggarwal et al. 2001) that takes into account the falloff in the corners of the images produced by a lens. The radiance filter implemented in Panotools (Senore 2004) was used in order to compensate this effect.

The following step (3rd) supposes a refinement of the previous ones. It is based on the visual correlation between the overlapped images and allows the alignment of the photographs taken by identifying significant points between pairs of images (D'Angelo et al. 2007). This process is a stand-alone mosaicing method. Nevertheless, it is not very advisable or efficient considering the large collection of images that the algorithm has to
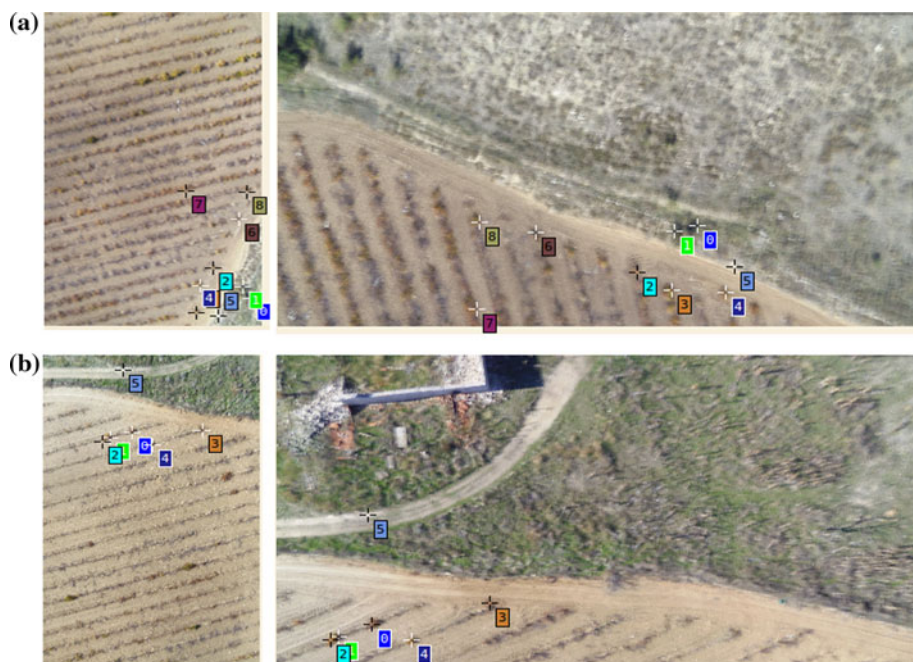

Fig. 12 Two examples of pairs of images related by control points. The *highlighted points* have been selected by SIFT algorithm and used in order to determine relative rotation between the related images

deal with. Furthermore, low visual disparity (the pictures are quite similar) makes the process even more time-consuming without the capability of providing an unambiguous solution.

However, complexity would be exponentially reduced if the alignment process were only applied to the images found in a reduced area. In such manner, the algorithm tries only to match neighboring images, structured in this way according to the results of the previous steps. Thus, only a local search is required, focusing on the adjacent borders. The coincidences found define a concrete relation (orientation, location and perspective) between each pair of images. It enables the algorithm to adjust both the EV and the orientation of the images, considering both areas as homogeneous from that moment.

The uniform area increases its size for each iteration until the entire field is considered. Nevertheless, there is also a secondary global post process which considers the relation between photographs in a global way. This technique allows reducing exaggerated distortions in the last images which have been derived from a daisy chain distortion transmission. Using this algorithm, the fine adjustment of the orientation for each image is sped up and it thereby reduces failure rate.

The two horizontal examples presented in Fig. 12 illustrate how the control-points search method works: Based on the scale-invariant feature transform algorithm (Lowe 1999; Ke and Sukthankar 2004), the program correlates similar (identical) physical features in order to establish the relative camera orientations mathematically.

In the last step, visually-enhanced algorithms have been used for improving the mosaic quality and fusion. The manual adjustment of sharpening, contrast and color temperature has allowed highlighting of the crop rows and plants in the scenario. It makes characteristic recognition easier. Softening and blurring algorithms have been also applied in order to smooth the borders between images. Figure 13 shows the final composition after implementing these techniques. It should be considered that the inner area without coverage (highlighted with the red circle) is the area prohibited in the path planning. Absence of data is thereby fully justified.

Fig. 13 Final composition after applying the visual enhancing algorithms

Fig. 14 Comparison between the generated image and the expected one, provided by a GIS system

Finally, as a verification process, the resulting image has been compared with the one expected (provided by other GIS systems). In this case, a matching process has been carried out with the satellite image (see Fig. 14). It has allowed a fine adjustment in the geo-referencing of the mosaic. Thus, some minor errors in the perspective, due to bias in the calibration of the system, have also been corrected.

Conclusions

In this paper, a complete tool that allows aerial image mosaicing with low cost components has been presented. A novel path-planning tool, which produces near-optimal trajectories applicable to many different commercial UAVs, has been developed. A detailed study of the main problems in selecting and installing the cameras onboard has been carried out. A complete mission definition example has also been provided. Experimental results including reliable and fast mosaicing procedures have been presented.

This study proves that a complete aerial image of a large area can be obtained by using small UAVs in a fast, affordable and reliable way.

MachinismeAgricole, du Gènie Rural, des Eaux et des Forets -CEMAGREF, CNH Belgium NV, CNH France SA, Bluebotics S.A. y CM Srl.

References

Aggarwal, M., Hua, H., Ahuja, N. (2001). On cosine-fourth and vignetting effects in real lenses. In B. Werner (Ed.), *Proceedings of the eighth international conference on computer vision* (Vol. 1, pp. 472–479). Vancouver: IEEE Computer Society.

Berni, J., Zarco-Tejada, P., Suarez, L., & Fereres, E. (2009). Thermal and narrowband multispectral remote sensing for vegetation monitoring from an unmanned aerial vehicle. *Geoscience and Remote Sensing, IEEE Transactions, 47*(3), 722–738.

Choset, H. (2001). Coverage for robotics—A survey of recent results. *Annals of Mathematics and Artificial Intelligence, 31*(1–4), 113–126.

D'Angelo, P. (2012). Radiometric alignment and vignetting calibration. In K. D. Baker et al. (Eds.), *Proceedings 5th international conference on computer vision systems*. Bielefeld: Applied Computer Science Group.

German, D., D'Angelo, P., Gross, M., & Postle, B. (2007). New methods to project panoramas for practical and aesthetic purposes. In D. W. Cunningham, G. Meyer, L. Neumann, A. Dunning, R. Paricio (Eds.), *Proceedings of computational aesthetics, Baff, Canada* (pp. 15–22). Aire-la-Ville: Eurographics Association.

Herwitz, S., Johnson, L., Dunagan, S., Higgins, R., Sullivan, D., Zheng, J., et al. (2004). Imaging from an unmanned aerial vehicle: Agricultural surveillance and decision support. *Computers and Electronics in Agriculture, 44*(1), 49–61.

Hunt, E. R., Hively, W. D., Fujikawa, S. J., Linden, D. S., Daughtry, C. S. T., & McCarty, G. W. (2010). Acquisition of nir-green-blue digital photographs from unmanned aircraft for crop monitoring. *Remote Sensing, 2*(1), 290–305.

Jiao, Y.S.,Wang, X.M., Chen, H., & Li, Y. (2010). Research on the coverage path planning of uavs for polygon areas. In Jing Bing Zhang et al. (Eds.), *Proceedings of the 5th IEEE conference on industrial electronics and applications* (pp. 1467–1472). Piscataway, New Jersey, USA: IEEE Service Center.

Johnson, L.F., Herwitz, S., Dunagan, S., Lobitz, B., Sullivan, D., & Slye, R. (2003). Collection of ultra high spatial and spectral resolution image data over California vineyards with a small uav. In International Center for Remote Sensing of Environment (Ed.), *Proceedings of the international symposium on remote sensing of environment* (pp. 221–230). Honolulu, HI: International Center for Remote Sensing of Environment.

Ke, Y., & Sukthankar, R. (2004). Pca-sift: A more distinctive representation for local image descriptors. In *proceedings of the 2004 IEEE computer society conference on computer vision and pattern recognition* (Vol. 2, pp. II–506). Washington: IEEE.

LaValle, S. M. (2006). *Planning algorithms*. Cambridge: Cambridge University Press.

Lelong, C. C. D., Burger, P., Jubelin, G., Roux, B., Labbe, S., & Baret, F. (2008). Assessment of unmanned aerial vehicles imagery for quantitative monitoring of wheat crop in small plots. *Sensors, 8*(5), 3557–3585.

Lowe, D. (1999). Object recognition from local scale-invariant features. In B. Werner (Ed.), In *The proceedings of the seventh IEEE international conference on computer vision* (Vol. 2, pp. 1150–1157). IEEE. doi:10.1109/ICCV.1999.790288.

Maza, I., & Ollero, A. (2007). Multiple uav cooperative searching operation using polygon area decomposition and efficient coverage algorithms. In R. Alami, R. Chatila, H. Asama (Eds.), *Distributed autonomous robotic systems* (Vol. 6, pp. 221–230). Tokyo: Springer.

Nebiker, S., Annen, A., Scherrer, M., & Oesch, D. (2008). A light-weight multispectral sensor for micro uav—opportunities for very high resolution airborne remote sensing. *The International Archives of the Photogrammetry, Remote Sensing and Spatial Information Sciences, XXXVII*, 1193–1200.

Philpot, W. (2001). *Digital image processing*. Ithaca: Cornell University.

Quigley, M., Gerkey, B., Conley, K., Faust, J., Foote, T., Leibs, J., Berger, E., Wheeler, R., & Ng, A. (2009). Ros: an open-source robot operating system. In *Proceedings of the IEEE international conference on robotics and automation (workshop on open source software)*. Kobe.

Senore, F. (2004). Accessed September 2, 2012 from http://wiki.panotools.org/Fluvio_Senore.

Valente, J., Barrientos, A., Cerro, J. D., & Sanz, D. (2011a). A waypoint-based mission planner for farmland coverage with an aerial robot—A precision farming tool. In J. V. Stafford (Ed.), *Proceedings of the 8th*

european conference on precision agriculture (pp. 427–436). Wageningen: Wageningen Academic Publishers.

Valente, J., Sanz, D., Barrientos, A., Cerro, Jd., Ribeiro, A., & Rossi, C. (2011b). An air-ground wireless sensor network for crop monitoring. *Sensors, 11*(6), 6088–6108.

Xiang, H., & Tian, L. (2011). Method for automatic georeferencing aerial remote sensing (RS) images from an unmanned aerial vehicle (uav) platform. *Biosystems Engineering, 108*(2), 104–113.